Analysis of the Gal-Chen–Zhang Single-Doppler Velocity Retrieval

STEVEN LAZARUS, ALAN SHAPIRO, AND KELVIN DROEGEMEIER

School of Meteorology, University of Oklahoma, Norman, Oklahoma

(Manuscript received 28 July 1997, in final form 9 January 1998)

ABSTRACT

The authors present herein an analysis of a single-Doppler velocity retrieval (SDVR) technique whereby the unobserved wind components are determined from single-Doppler radar data. The analysis is designed to provide information about the behavior and/or sensitivity of the SDVR scheme as a function of various internal and external parameters as well as about observational errors and weights.

Results presented for retrieval of both the mean and local flow indicate that the SDVR breaks down if the reflectivity gradient vanishes or if a reflectivity isoline is locally perpendicular to the radar beam. In the absence of reflectivity or radial velocity errors, the mean flow solution is independent of the integration area, the radar location, the signal wavenumber, and the weights. Given perfect radial wind information, error in the reflectivity field degrades the solution. Contrary to the error-free solution, the solution with error depends on the integration area.

Error statistics indicate that radial wind information alone is not sufficient to retrieve the local wind. Reduced error norms reveal that an optimal (i.e., reduced error norms) integration area exists that is dependent upon the length of time between radar volume scans, suggesting that the velocity field is *not* stationary (as was assumed) over these scans.

1. Introduction

The demands of convective-scale research will likely necessitate the use of data from sources such as Doppler radars, surface mesonet stations, and wind profilers. Doppler radar provides the most comprehensive observations in terms of space and time resolution, but, unfortunately, a single radar measures only the radial wind component (and reflectivity) in a three-dimensional (3D) volume. The paucity of high-resolution 3D measurements of the vector wind field is potentially problematic in the context of convective-scale initialization and prediction. For example, in the research community, some forward data assimilation techniques employ a thermodynamic recovery procedure that retrieves the pressure and buoyancy fields from the equations of motion via a least squares method that yields a Poisson equation for pressure (Gal-Chen 1978). It has been shown, however, that in order to arrive at accurate estimates of the pressure and buoyancy fields, the Gal-Chen technique requires knowledge of the *three-dimensional* wind and its time tendency (Hane et al. 1981; Crook 1994). To complicate matters further, the radial wind field is not known everywhere, and large data voids frequently exist within an analysis volume.

Corresponding author address: Dr. Steven Lazarus, Department of Meteorology, University of Utah, 819 Wm. C. Browning Bldng, Salt Lake City, Utah 84112.
E-mail: slazarus@atmos.met.utah.edu

The challenge to produce a dynamically consistent and complete set of initial conditions suitable for a numerical forecast on the storm scale has led to the development of techniques known as single-Doppler velocity retrieval (SDVR). Employed as an independent algorithm, SDVR also has the potential to improve both nowcasting and hazard warning. Although SDVR techniques vary in complexity, from simple conservation principles to the use of full dynamic constraints, each is employed to assist in the recovery of the cross-beam (azimuthal) and vertical (polar) wind components. For example, Shapiro et al. (1995) apply a two-scalar conservation technique whereby reflectivity and a second derived scalar field are used to recover the 3D boundary layer wind field. Weygandt et al. (1995) extend the Shapiro technique to a deep-convective dataset. Using a variational approach whereby a single Cartesian wind component was assumed known, Liou et al. (1991) adjust (retrieve) the other two model components subject to a constraint that minimizes the divergence of the adjusted plus the observed winds. Xu et al. (1995) utilize the adjoint technique to retrieve microburst winds from single-Doppler data. Sun et al. (1991) also employ the adjoint methodology to retrieve both wind and temperature fields using a single wind component from model-simulated data. Her method was then adapted to directly incorporate simulated radial velocity information instead of a single Cartesian component (Sun 1994). Tuttle and Foote (1990) retrieve the two-dimensional (2D) boundary layer flow from a single Doppler by utilizing

a correlation technique known as tracking radar echoes by correlation (TREC). Crook and Tuttle (1994) also use the TREC method to determine the boundary layer winds in association with three observed gust front cases.

This paper focuses on a particular SDVR technique that utilizes a least squares method proposed by Gal-Chen and Zhang (1993, hereafter GZ). The simple nature of the GZ retrieval allows for an analytic analysis that is not easily obtainable with other SDVR techniques. The advantage of such an analysis lies in its potential to provide a priori information about the behavior and/or sensitivity of the scheme as a function of various internal and external parameters as well as the sensitivity of the scheme to the observations themselves (e.g., weights, radius of influence, errors). Albeit somewhat idealized, the work presented here has been designed to provide insight with respect to the application of the GZ scheme to real data.

The GZ algorithm, discussed briefly in section 2, retrieves the 3D wind field from multiple time levels of radar data by assuming that, in the absence of source terms (e.g., precipitation fallout, coalescence, evaporation, etc.), reflectivity is conserved and that the velocity field is stationary in a frame of reference that moves with the mean translation speed of the reflectivity field. The velocity vectors obtained from the retrieval satisfy, in a least squares sense, the Eulerian equation for reflectivity conservation and a second weak constraint whereby their projection in the direction of the radial wind is approximately equal to that of the observed radial wind. In sections 3 and 4, we present the results of a constant wind retrieval with and without error in the input (simulated) reflectivity field. Section 5 details a local flow retrieval in which the idealized zonal velocity varies as a linear function of x. A summary and conclusions are presented in section 6.

2. Overview of the SDVR technique

Instead of enforcing only reflectivity (Z) conservation exactly (e.g., Qiu and Xu 1992), we also enforce the geometric constraint relating the radial velocity to the Cartesian velocity components in a least squares sense (as weak constraints) by minimizing the functional,

$$J \equiv \int_{\mathbf{x},t} \left\{ \mu \left[\frac{\partial Z}{\partial t} + u\frac{\partial Z}{\partial x} + v\frac{\partial Z}{\partial y} + (w + W_t)\frac{\partial Z}{\partial z} \right]^2 + \left[v_r - u\frac{x - x_0}{r} - v\frac{y - y_0}{r} - (w + W_t)\frac{z - z_0}{r} \right]^2 \right\} d\mathbf{x}\, dt, \quad (1)$$

where $d\mathbf{x}$ is a 2D (x, y) increment; dt is the time increment; u, v, and w are the advection velocities; x, y, and z are the coordinates of the observations; W_t is the terminal velocity of the precipitation particles; v_r is the radial velocity; x_0, y_0, and z_0 are the x, y, and z coordinates of the radar; and r is the radar-to-gridpoint distance given by

$$r = [(x - x_0)^2 + (y - y_0)^2 + (z - z_0)^2]^{1/2}. \quad (2)$$

Note that all quantities in (1) are given in a *fixed* reference frame. A detailed description of the derivation of (1) in a moving reference frame is given in Zhang and Gal-Chen (1996, hereafter GZ96). The weight μ is given as a ratio of the reflectivity-to-radial velocity weights, both of which are determined from their inverse variances, that is,

$$\mu = \frac{1/\sigma_z^2}{1/\sigma_{v_r}^2} = \frac{\displaystyle\int_{\mathbf{x},t} 1/(Z_t - \overline{Z}_t)^2 f(Z_t)\, d\mathbf{x}\, dt}{\displaystyle\int_{\mathbf{x},t} 1/(v_r - \overline{v}_r)^2 f(v_r)\, d\mathbf{x}\, dt}, \quad (3)$$

where the overbar denotes a mean value, the subscript t indicates a derivative with respect to time, and $f(Z_t)$ and $f(v_r)$ represent probability density functions. The weight μ is chosen so as to ensure that each constraint in (1) has the same order of magnitude, $\overline{Z}_t$ and $\overline{v}_r$ are taken to be zero, and $f(Z_t)$ and $f(v_r)$ are set to one.

Equation (1) is minimized by differentiating J with respect to the three unknowns—u, v, and w—and setting the resulting equation equal to zero. This results in a system of three linear equations that can be written in matrix form as

$$\begin{bmatrix} a_{11} & a_{12} & a_{13} \\ a_{21} & a_{22} & a_{23} \\ a_{31} & a_{32} & a_{33} \end{bmatrix} \begin{bmatrix} u \\ v \\ w \end{bmatrix} = \begin{bmatrix} b_1 \\ b_2 \\ b_3 \end{bmatrix}. \quad (4)$$

In practice, the coefficients a_{ij} are determined from the observed reflectivity and radial velocity fields,

$$a_{11} = \int_{\mathbf{x},t} \left\{ \mu \left(\frac{\partial Z}{\partial x} \right)^2 + \left(\frac{x}{r} \right)^2 \right\} d\mathbf{x}\, dt,$$

$$a_{12} = a_{21} = \int_{\mathbf{x},t} \left\{ \mu \frac{\partial Z}{\partial x}\frac{\partial Z}{\partial y} + \frac{xy}{r^2} \right\} d\mathbf{x}\, dt,$$

$$a_{22} = \int_{\mathbf{x},t} \left\{ \mu \left(\frac{\partial Z}{\partial y} \right)^2 + \left(\frac{y}{r} \right)^2 \right\} d\mathbf{x}\, dt,$$

$$a_{13} = a_{31} = \int_{\mathbf{x},t} \left\{ \mu \frac{\partial Z}{\partial x}\frac{\partial Z}{\partial z} + \frac{xz}{r^2} \right\} d\mathbf{x}\, dt,$$

$$a_{33} = \int_{\mathbf{x},t} \left\{ \mu \left(\frac{\partial Z}{\partial z} \right)^2 + \left(\frac{z}{r} \right)^2 \right\} d\mathbf{x}\, dt, \quad \text{and}$$

$$a_{23} = a_{32} = \int_{\mathbf{x},t} \left\{ \mu \frac{\partial Z}{\partial y}\frac{\partial Z}{\partial z} + \frac{yz}{r^2} \right\} d\mathbf{x}\, dt, \quad (5)$$

where we have neglected the terminal velocity and assumed that the radar is located at the grid origin (0, 0, 0). The right-hand-side forcing is given by,

$$b_1 = \int_{\mathbf{x},t} \left(-\mu \frac{\partial Z}{\partial x} \frac{\partial Z}{\partial t} + v_r \frac{x}{r} \right) d\mathbf{x}\, dt,$$

$$b_2 = \int_{\mathbf{x},t} \left(-\mu \frac{\partial Z}{\partial y} \frac{\partial Z}{\partial t} + v_r \frac{y}{r} \right) d\mathbf{x}\, dt, \quad \text{and}$$

$$b_3 = \int_{\mathbf{x},t} \left(-\mu \frac{\partial Z}{\partial z} \frac{\partial Z}{\partial t} + v_r \frac{z}{r} \right) d\mathbf{x}\, dt. \tag{6}$$

It is important to point out that, in the GZ96 technique, the *mean flow* (used to define the motion of the retrieval reference frame) is obtained by integrating the coefficients given in (5) and (6) over an entire *volume* (or as a function of height by integrating over all reflectivity and radial wind data at a given level), while the *perturbation flow* is obtained by integrating (5) and (6) over a *local* horizontal area. The total flow is then obtained by adding the perturbation flow onto the mean. In either case, the 3D winds can be retrieved by inverting (4), for example, by using Gaussian elimination.

Although we do not seek a solution in a moving reference frame when deriving the following analytic solutions, it should be used when GZ is applied to real data. In that case, the fixed frame estimate of the reflectivity time derivative may contain significant error resulting from aliasing due to the discrete nature of the finite difference formulation. For example, if a radar samples the reflectivity every 200 s, then a mean flow velocity as little as 1 m s^{-1} on a 200-m grid can lead to aliasing. Because the GZ mean flow velocities are retrieved by minimizing the variance in the reflectivity time derivative, the impact of retrieval errors due to aliasing can be mitigated by performing the retrieval in the moving frame. Additionally, the velocity stationarity assumption is least violated in a frame of reference moving with the principal features of interest. To define a moving reference frame, however, one must first retrieve the mean flow, and herein lies the impetus for this work. The experiments presented in this paper, which include an error impact analysis on the mean flow only, are primarily designed to examine the sensitivities of the mean flow GZ retrieval.

3. Mean flow retrieval with perfect observations

The GZ scheme given by (1) can be applied to retrieve the mean or total flow. In practice, one first obtains the mean flow, which is then used to define a moving reference frame and to solve for the perturbation flow velocity in the moving frame. The total flow is then obtained by adding the mean flow onto the perturbation velocity (GZ96). Because an accurate retrieval of the total flow depends upon a quality estimate of the mean flow, we will first examine the sensitivity of the GZ scheme with respect to an analytic mean flow solution. It is important to point out that estimates of the mean translation speed via (1) may vary depending on the specified domain size *R*. Although we vary *R* as well as the domain location relative to the radar (as shown in Fig. 1), the results presented in this section remain that of a mean flow retrieval in which just one pair of mean wind values (*U, V*) is obtained.

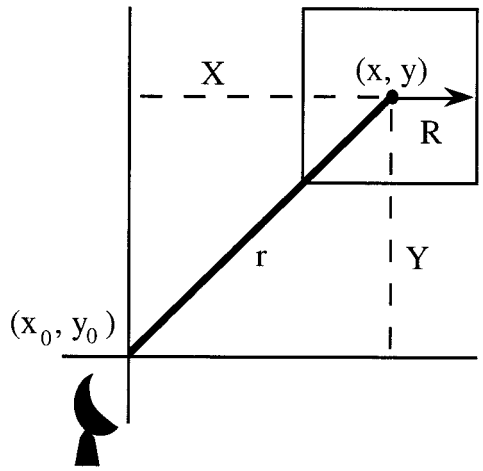

FIG. 1. Horizontal cross section indicating the relationship between the radar location (x_0, y_0), grid point (x, y), and the transformed variables (X, Y).

We consider the simple one-dimensional (1D) case of a sinusoidal reflectivity pattern of the form

$$Z(x, t) = \alpha \sin[k(x - Ut)] + \varepsilon(x), \tag{7}$$

where α and k are the signal amplitude and wavenumber, respectively, and U is the mean zonal velocity component of the true wind $\mathbf{v} = U\mathbf{i}$. Because observations are generally imperfect, we introduce a simple error term, $\varepsilon(x)$, defined as

$$\varepsilon(x) = \beta \sin(mx), \tag{8}$$

where β and m are the noise amplitude and wavenumber, respectively. We choose $\alpha = 10$ dBZ, $\lambda_x(2\pi/k) = 2500$ m, and $\varepsilon = 0$ so as to be representative of optically clear convective-scale boundary layer values. Note that (7) will not satisfy the 1D mean flow reflectivity conservation equation,

$$\frac{\partial Z}{\partial t} + U \frac{\partial Z}{\partial x} = 0, \tag{9}$$

unless $\varepsilon(x) = 0$.

Initially assuming that (8) is zero (i.e., no error), we substitute (7) into (5) and (6) and integrate over (x, y, t), with $z = 0$ and μ assumed to be constant (see appendix A for the coefficients). Due to the simple nature of our

assumed analytic solution, (4) reduces to two equations in two unknowns, that is,

$$a_{11}u^r + a_{12}v^r = Ua_{11} \quad \text{and}$$
$$a_{12}u^r + a_{22}v^r = Ua_{12}, \tag{10}$$

where u^r and v^r are the (unknown) Cartesian velocities to be retrieved. We reduce (10) to one equation and one unknown, that is,

$$\left(a_{12} - \frac{a_{11}}{a_{12}}a_{22}\right)v^r = 0. \tag{11}$$

There is only one solution to (11) as the coefficients a_{ij} are given to us from the observations. If the term enclosed by parentheses is not zero, then v^r must be equal to zero and we arrive at the desired mean flow solution, $u^r = U$. If the term enclosed by parentheses is zero or in practice becomes too small, then v^r blows up; that is, the solution becomes singular. This case interests us as it will shed light on the conditions under which the GZ scheme will fail to recover the mean flow.

If the parenthetical term is zero, then we must have

$$a_{12}^2 = a_{11}a_{22}. \tag{12}$$

To simplify the analysis, we evaluate the coefficients a_{11} and a_{22} at a *single point* in the observed flow field. Applying (5) in (12) (with $\partial Z/\partial y = 0$), we obtain

$$\frac{x^2y^2}{r^4} = \frac{y^2}{r^2}\left[\mu\left(\frac{\partial Z}{\partial x}\right)^2 + \left(\frac{x}{r}\right)^2\right]. \tag{13}$$

Therefore, (12) is satisfied exactly (and the solution breaks down) if $\partial Z/\partial x = 0$ or $y = 0$. *The former implies that one cannot retrieve the mean flow in regions where the reflectivity gradient vanishes.*

This problem also appears in the case of 2D flow with reflectivity conservation and the radial wind equation (i.e., $rv_r + ux + vy + wz = 0$) applied as strong constraints. The reflectivity conservation and radial wind equations form a system of two equations in two unknowns and therefore can be solved directly, yielding the following:

$$u^r = \frac{yZ_t + rv_rZ_y}{xZ_y - yZ_x} \quad \text{and} \quad v^r = \frac{xZ_t + rv_rZ_x}{xZ_y - yZ_x}, \tag{14}$$

where the subscripts x, y, and t denote derivatives with respect to space (x, y) and time t. The denominator in (14), which is the scalar triple product $\mathbf{k} \cdot (\mathbf{r} \times \nabla Z)$, indicates that a singularity will occur if the reflectivity gradient vanishes *or* if a reflectivity isoline is locally perpendicular to the radar beam. These problems are similar to those encountered by other advective retrieval techniques that employ scalar conservation relationships (e.g., Shapiro et al. 1995). They can, however, be mitigated by expanding the integration domain in space and by using information over multiple time levels (e.g., Qiu and Xu 1992). Outside of these regions, the mean flow can be retrieved and in the absence of reflectivity or radial velocity error, the GZ mean flow solution is independent of the area of integration R, radar location (x_0, y_0), signal wavenumber k, and weight μ.

4. Mean flow retrieval with error

a. Theory

For the idealized 1D problem just described in which error-free data were assumed, regions where $\partial Z/\partial x$ vanish correspond to those where $\partial Z/\partial t$ vanish. Unfortunately, this will not generally be the case as real data typically contain error. Because errors associated with the reflectivity conservation constraint will generally be much larger than those associated with the radial wind constraint, tests in which the radial wind error is zero are both interesting and legitimate. In this section, we consider the impact of reflectivity field error on the mean flow retrieval presented above.

When (8) is nonzero, the numerical values of a_{11} and b_1 must be modified from those in the previous section to allow for the presence of error. Because of the additional terms, (9) is no longer satisfied. Each of these coefficients has additional terms that arise from the x gradient in Z, and for a_{11} we have the addition of two terms, that is,

$$\left(\frac{\partial Z}{\partial x}\right)^2 = \left(\left.\frac{\partial Z}{\partial x}\right|_{\varepsilon=0} + \frac{\partial \varepsilon}{\partial x}\right)^2$$
$$= \left(\left.\frac{\partial Z}{\partial x}\right|_{\varepsilon=0}\right)^2 + 2\frac{\partial \varepsilon}{\partial x}\left.\frac{\partial Z}{\partial x}\right|_{\varepsilon=0} + \left(\frac{\partial \varepsilon}{\partial x}\right)^2, \tag{15}$$

where $\varepsilon = 0$ indicates the evaluation of (7) with $\varepsilon(x) = 0$. Only one additional term is needed for b_1, that is,

$$\left(\frac{\partial Z}{\partial x}\frac{\partial Z}{\partial t}\right) = \left(\left.\frac{\partial Z}{\partial t}\frac{\partial Z}{\partial x}\right|_{\varepsilon=0} + \frac{\partial Z}{\partial t}\frac{\partial \varepsilon}{\partial x}\right). \tag{16}$$

Substituting the analytic value for Z with error ε and integrating over space and time yields a modified a_{11} and b_1 [see (B1) and (B2) in appendix B for more details]. Because the error term is a function of x only, the remaining coefficients do not change. Note that the mean flow solution now depends on the error amplitude β and wavenumber m.

As discussed previously, if $\varepsilon = 0$ and the x gradient of Z does not vanish, we are guaranteed to retrieve the mean flow *exactly* even when using a single point instead of an area average provided that $(\mathbf{r} \times \nabla Z) \neq 0$. However, even if the latter holds, the inclusion of an error term, as specified by (8), yields retrieved mean flow velocities that can vary from the true solution. For example, via Gaussian elimination, (4) yields

$$v^r = \mu(\varepsilon_{b_1} - U\varepsilon_{a_{11}})/d, \tag{17a}$$

where ε_{b_1} and $\varepsilon_{a_{11}}$ denote the error terms given in ap-

pendix B and d is a combination of the coefficients a_{ij} and weight μ given by

$$d = a_{12} - \frac{a_{22}}{a_{12}}\{\mu[a_{11}(Z) + \varepsilon_{a_{11}}] + a_{11}(v_r)\}. \quad (17b)$$

The coefficient a_{11} in (17b) has been partitioned with respect to contributions from the reflectivity Z and radial wind v_r equations [i.e., the first and second terms of the a_{11} integrand (5), respectively]. The impact of this error term on the retrieved wind will depend on the signal-to-noise amplitude and wavelength (see section 4b). Equation (17a) indicates that, in the presence of reflectivity error, a judicious choice of weights can mitigate (or remove) these errors. Here, setting $\mu = 0$ would produce the correct retrieval (i.e., $u^r = U$ and $v^r = 0$). Hence, given perfect radial velocity information, any error (no matter how slight) in the reflectivity field degrades the mean flow solution. Under these circumstances, the retrieval performs better without any reflectivity information.

For the case where we have perfect reflectivity and imperfect radial winds, the error terms are not coupled to the weights as in (17a) and (17b). For example, if we add an error term onto the radial wind in a manner similar to that for the reflectivity as specified by (7), that is, $v_r = v_r + \varepsilon(x)$, we have

$$v^r = \frac{\int_{\mathbf{x},t}\left[\varepsilon(x)\frac{x}{r}\right] d\mathbf{x}\, dt - \frac{a_{11}}{a_{12}}\int_{\mathbf{x},t}\left[\varepsilon(x)\frac{y}{r}\right] d\mathbf{x}\, dt}{d'}, \quad (18)$$

where d' is given by (17b) with $\varepsilon_{a_{11}} = 0$ and $\varepsilon(x)$ is an error term. In the limit in which μ approaches infinity (i.e., the reflectivity constraint is given increasing weight), (18) reduces to

$$v^r = \frac{\int_{\mathbf{x},t}\left[\varepsilon(x)\frac{y}{r}\right] d\mathbf{x}\, dt}{a_{22}}. \quad (19)$$

Consequently, v^r does not approach zero unless $\varepsilon(x)$ approaches zero or $a_{22} \gg \int\{\varepsilon(x)y/r\}$.

b. Results

Figure 2 shows the mean flow analytic retrieval for a series of experiments (of varying weights μ) in a 40 km × 40 km domain with mean flow $U = 20$ m s^{-1}, noise amplitude $\beta = 5.0$ dBZ (the equivalent of 50% amplitude error as the signal amplitude α is set to 10 dBZ), $t = 100$ s, $R = 1000$ m, and the signal wavelength $\lambda_x = 2500$ m. These values were selected to facilitate comparison with the error-free mean flow retrieval in section 3. The three curves represent mean vector error as a function of μ for noise wavelengths ($\lambda_m = 2\pi/m$) ranging from less than that of the signal (628 m) to greater than that of the signal (3142 and 6283 m). We

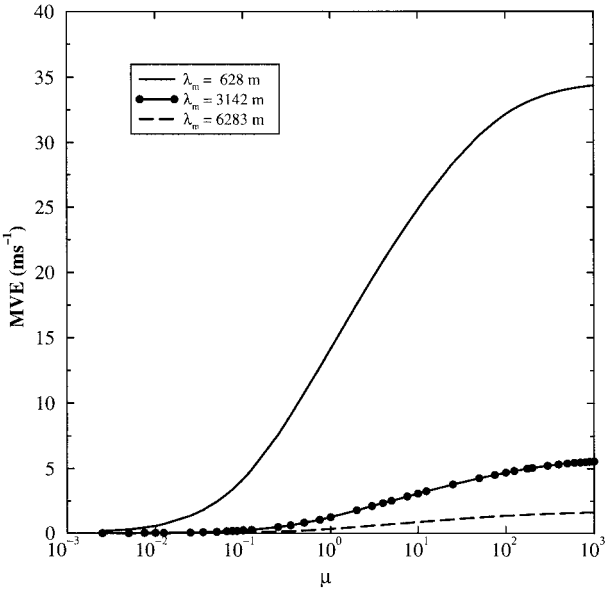

FIG. 2. Log-linear graph of the mean flow with error analytic solution to GZ. Each curve represents the MVE (domain averaged over a 40 km × 40 km domain) for a series of experiments as a function of μ, for varying noise wavelengths (λ_m) of 628 m (solid curve), 3142 m (solid curve with circles), and 6283 m (dashed curve). All other parameters are fixed, including mean flow, $U = 20$ m s^{-1}, signal-to-noise amplitude, $\alpha/\beta = 2.0$ (the equivalent of 50% amplitude error), $t = 100$ s, $R = 1000$ m, and signal wavelength $\lambda_x = 2500$ m.

retrieve the wind over a given region in the x–y plane where x and y are confined to be greater than zero with respect to the radar. At each point we calculate the vector error and then sum over all the points to obtain the mean vector error (MVE) using

$$\text{MVE} = \frac{1}{N}\sum_{j=1}^{ny}\sum_{i=1}^{nx}\left[(u^r_{i,j} - U)^2 + (v^r_{i,j} - V)^2\right]^{1/2}, \quad (20)$$

where N ($=nx \times ny$) is the total number of points (1681) and nx and ny are the number of points in the x and y directions, respectively. A perfect retrieval (i.e., MVE = 0.0) implies that $u^r_{i,j} = U$ and $v^r_{i,j} = 0$ at each of these points. Regardless of the choice of λ_m, as μ approaches zero, that is, as the reflectivity equation in (1) is given less weight, we obtain the exact solution (i.e., the MVE approaches zero) for the retrieved mean flow ($U = 20$ m s^{-1}, $V = 0.0$ m s^{-1}). For the case of the constant wind, in the presence of perfect radial wind information and a reflectivity field containing error, one should omit the reflectivity constraint altogether, as (17a) above suggests.

Except for values of weights near $\mu = 0$, where the MVE approaches zero, the MVE values are slowly varying for a broad selection of weights (recall Fig. 2 is a log-linear plot). Estimates of the weights determined from (3) are typically on the order of 10^3 m^2 dBZ^{-2} or greater and consequently fall outside of the region where the MVE values increase steeply as a function of μ.

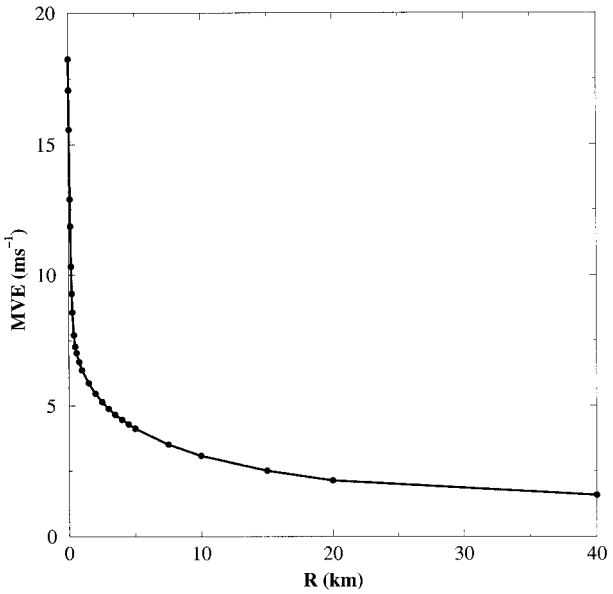

FIG. 3. Mean flow with error analytic solution to GZ. Each dot on the curve represents the domain MVE as a function of the integration area R for fixed $U = 20$ m s^{-1}, $\alpha/\beta = 5.0$ (the equivalent of 20% amplitude error), $t = 100$ s, and $\lambda_x = 2500$ m. Here, μ is determined from Eq. (3).

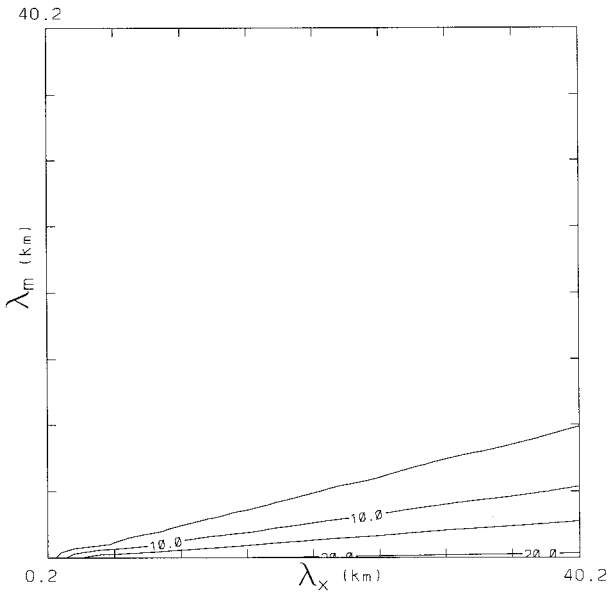

FIG. 4. Mean flow with error analytic solution to GZ. Contours of domain MVE as a function of λ_x and λ_m. Here, R is fixed at 40 km, $U = 20$ m s^{-1}, $\alpha/\beta = 5.0$, and $t = 100$ s. Here, μ is determined from Eq. (3). The contour interval is 5 m s^{-1}.

Thus, even an order of magnitude change in μ has little impact on the MVE. This suggests that there will be little sensitivity to the choice of weights.

Because the error amplitude is fixed at 50% for each curve in Fig. 2, the large differences in the MVE can be attributed directly to the noise wavelength λ_m. The MVE approaches values twice that of the mean flow for $\lambda_m = 628$ m, indicating that short wavelength noise dominates the solution as rapidly varying reflectivity gradients overwhelm the more slowly varying gradients of the signal. As the wavelength of the noise increases to values larger than that of the signal, the MVE values decrease significantly (from 200% to 10%). The MVE can be reduced further by choosing R as large as possible (e.g., the entire domain)—a potentially desirable result that suggests one can mitigate the impact of observational errors by utilizing a larger horizontal domain.

This is demonstrated in Fig. 3, which shows the MVE for a series of experiments in which the signal and noise wavelengths and amplitudes are held fixed. As R approaches 40 km, the MVE decreases from 18 m s^{-1} to less than 2 m s^{-1}. This result is in direct contrast with the error-free mean flow solution, which was independent of R. The integration over a larger area effectively smoothes the noise by summing over a greater number of sinusoids so that there is some cancellation of the error term.

Figure 4 depicts the MVE for a series of retrievals in which the signal-to-noise wavelength is varied. Because of the previous finding, we take R to be relatively large—40 km. The mean wind U (20 m s^{-1}) is selected to be a value representative of a strong surface outflow, while α/β (5.0) is chosen such that the error magnitude is 20% of the signal amplitude. The integration period t (100 s) employed herein, albeit short, is comparable to the observed time between consecutive radar volume scans found in other boundary layer wind retrievals (e.g., Sun and Crook 1994, 1996; Xu et al. 1994; Shapiro et al. 1995) of radar data collected in the research mode. Note the impact of the short wavelength noise on the MVE as the error grows rapidly for decreasing noise wavelength and is largest when $\lambda_m/\lambda_x < 1$. In contrast, for λ_m/λ_x fixed at 0.5, the MVE is more uniformly distributed as a function of signal-to-noise (α/β) amplitude (Fig. 5). Even for $\alpha/\beta \approx 1$, error levels are only slightly greater than 50% (recall $U = 20$ m s^{-1}). The former figure suggests that large sensitivities exist for short wavelength noise, while the latter indicates large errors when $\beta \gg \alpha$.

In Fig. 6 we show the MVE as a function of noise amplitude β and noise wavenumber m ($\alpha = 10$ dBZ, $\lambda_x = 2500$ m, $t = 100$ s, and $R = 1.0$ km are fixed). It is important to point out that the scheme displays significant sensitivity to both high amplitude-to-long wavelength noise and low amplitude-to-short wavelength noise. This figure also demonstrates that if the noise amplitude is *small* (and fixed), changes in the noise wavelength will not greatly increase the MVE; conversely, if the noise wavelength is *large* (and fixed), changes in the noise amplitude will not significantly impact the MVE.

We can see this more clearly in Fig. 7, where the

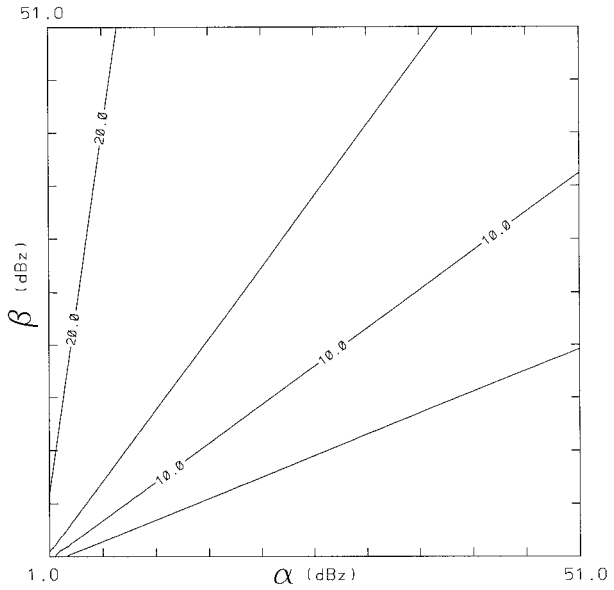

FIG. 5. Mean flow with error analytic solution to GZ. Contours of domain MVE as a function of α and β. Here, R is fixed at 40 km, $U = 20$ m s^{-1}, $\lambda_x/\lambda_m = 2.0$, and $t = 100$ s. Here, μ is determined from Eq. (3). The contour interval is 5 m s^{-1}.

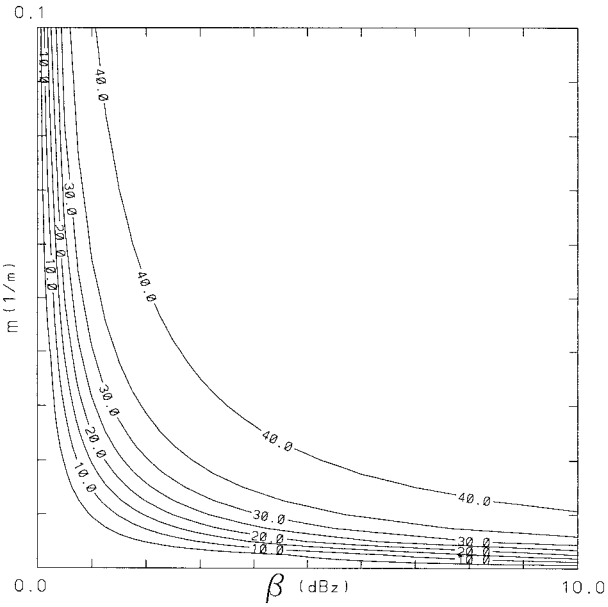

FIG. 6. Mean flow with error analytic solution to GZ. Contours of domain MVE as a function of β and noise wavenumber m. Here, R is fixed at 1 km, $U = 20$ m s^{-1}, $\lambda_x = 2500$ m, $\alpha = 10.0$ dBZ, and $t = 100$ s. Here, μ is determined from Eq. (3). The contour interval is 5 m s^{-1}.

MVE for five particular noise wavenumbers is displayed against the noise amplitude ($\alpha = 10$ dBZ, $\lambda_x = 2500$ m, $t = 100$ s, and $R = 1.0$ km are fixed). For error amplitudes approaching 50% of the signal, the errors are significantly reduced when the wavelength of the noise is less than that of the signal ($m < 0.0025$ or $\lambda_m/\lambda_x < 1$). These results suggest that selective filtering of small-scale noise (relative to the signal wavelength) may have a significant impact on reducing the error. Radar data that are collected using a high signal-to-noise threshold are likely to improve the quality of the retrieval. In practice, however, it is difficult to distinguish between noise and signal, and any attempt to remove short-wavelength noise invariably removes signal as well.

Displayed in Fig. 8 is an x–y cross section of the error in the retrieved v^r field. Here, $\beta = 5.0$ dBZ (50% amplitude error), $\lambda_m = 628.3$ m, $\lambda_x = 2500$ m, $R = 1.0$ km, and the weights are computed via (3). The errors (not shown) in the retrieved u component are near 80% (16 m s^{-1}) over most of the domain with only slight east-to-west variations due to the sinusoidal nature of the error term, which is x dependent only. As discussed above, the large errors are a result of the relatively small noise wavelength (628 m) compared to that of the signal (2500 m). While the error in the retrieved mean zonal flow is distributed evenly in the x–y plane, the mean meridional wind reveals a systematic error distribution. Here, we see that the error tends to align itself with the radar that is located at the origin (0, 0) of the domain (southwest of the lower left-hand corner).

The largest error occurs due east of the radar (i.e.,

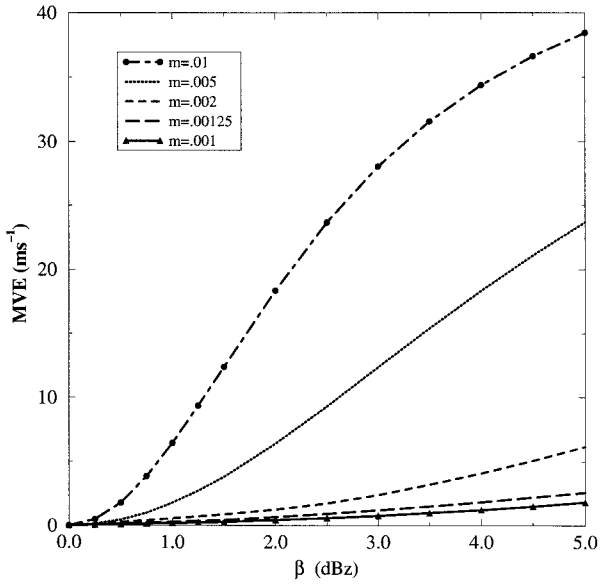

FIG. 7. Mean flow with error analytic solution to GZ. Each curve represents the MVE for a series of experiments as a function of β for varying m of 0.01 (dashed-dotted with circles), 0.005 (short dashed curve), 0.002 (medium dashed curve), 0.00125 (long dashed curve), and 0.001 (solid curve with circles). Here, R is fixed at 1 km, $U = 20$ m s^{-1}, $\lambda_x = 2500$ m, $\alpha = 10.0$ dBZ, and $t = 100$ s. Here, μ is determined from Eq. (3).

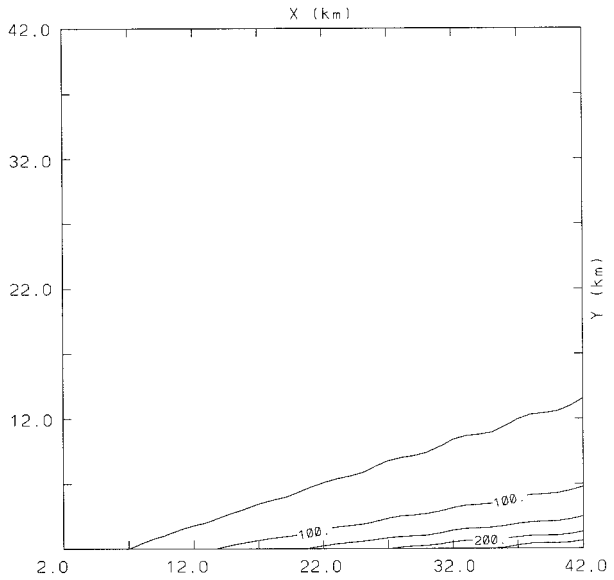

FIG. 8. Mean flow with error analytic solution to GZ. Horizontal cross section (at $z = 0$ m) of the v component error. Here, R is fixed at 1 km, $U = 20$ m s^{-1}, $\alpha/\beta = 2.0$, $\lambda_x/\lambda_m = 4.0$, and $t = 100$ s. Here, μ is determined from Eq. (3). The contour interval is 50 m s^{-1}.

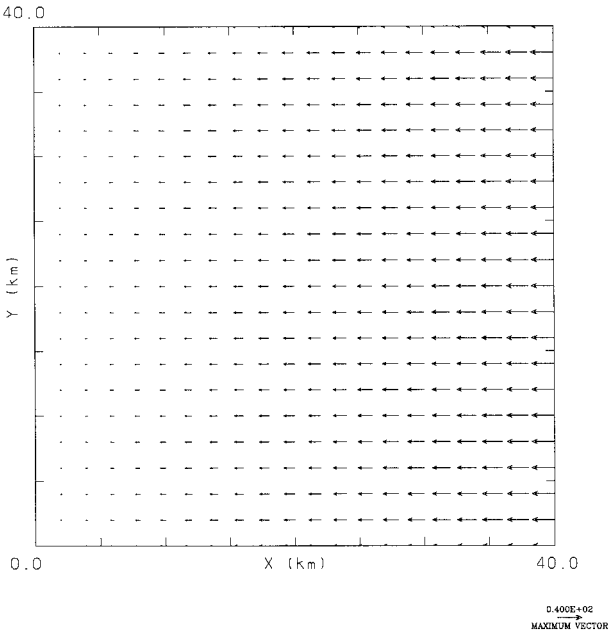

FIG. 9. Divergent flow solution to GZ. Horizontal cross section of the vector field (at $z = 0$ m) as determined from Eq. (23). Here, $C = 0.001$ s^{-1} and $t = 100$ s. Vectors are scaled by a maximum vector length of 40 m s^{-1}.

along the positive x axis) and decreases to the north and west. Although the ''true'' v component is zero, some of the retrieved values are quite large (i.e., in excess of 200 m s^{-1}). As discussed in section 3 for the error-free mean flow, the solution becomes singular due to the disappearance of the reflectivity gradient in the cross-beam (v^r) direction, that is, $(\mathbf{r} \times \nabla Z) = 0$. The retrieval of the cross-beam wind (u^r) along $x = 0$ does not produce a singularity because the cross-beam gradient exists (i.e., $\partial Z/\partial x \neq 0$) here. In the case in which the data are considered to be perfect (error free), the singularity problem exists at $y = 0$ only, and we are able to retrieve the exact mean flow at all other points in the domain. Here, the violation of reflectivity conservation, (9), due to the introduction of the error term yields a numerator in (14) that is no longer zero as it was for the error-free solution. Thus as the denominator $k \cdot (\mathbf{r} \times \nabla Z)$ approaches zero (at $y = 0$), the solution grows without bound. Also note that the nature of the solution indicates that v^r grows faster for larger x, hence explaining the slope of the MVE contours in Fig. 8.

The results presented here indicate that domainwide integration of (5) and (6) to retrieve the mean flow can possibly mitigate the influences of error in the reflectivity field (or errors due to the violation of the reflectivity conservation assumption, e.g., evaporation, condensation, precipitation fallout). However, real data is far more complex than these highly idealized solutions. Errors will be present in the radial velocity as well as the reflectivity field, and errors will not be independent of time as was assumed here. Nevertheless, these results do shed some valuable insight on the nature of the GZ scheme. In the next section, we examine a retrieval of a divergent flow.

5. Retrieval of a divergent flow

We now prescribe the reflectivity field,

$$Z = \alpha \sin[kx(1 + Ct)], \tag{21}$$

where C has units of frequency and the wavelength of Z is modulated by time t. Equation (21) exactly satisfies the conservation equation

$$\frac{\partial Z}{\partial t} + u\frac{\partial Z}{\partial x} = 0, \tag{22}$$

where

$$u = \frac{-Cx}{1 + Ct}. \tag{23}$$

The zonal velocity is a linear function of x and, for positive C, decreases from west to east across the domain (Fig. 9). Comparing (21) and (7) (where $\varepsilon = 0$) and recalling that v_r is obtained from (23) via $v_r = ux/r$, we see that the coefficients that are a function of either the x gradient in reflectivity or the radial wind will differ from those derived for the constant wind solution in

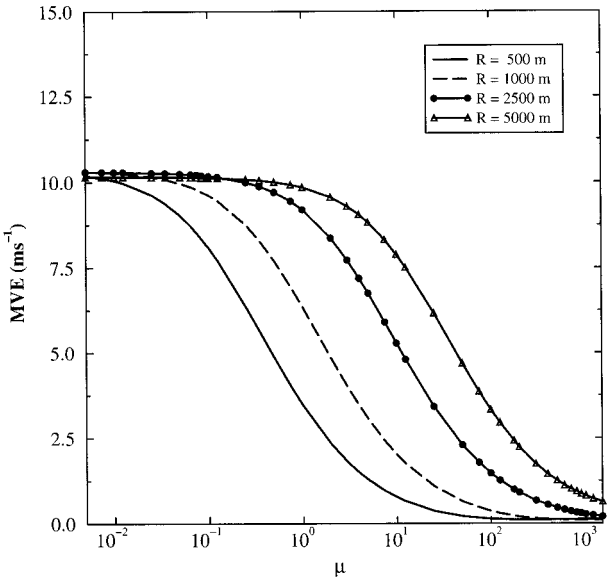

FIG. 10. Log-linear graph of the divergent flow solution to GZ. Each curve represents the domain MVE for a series of experiments as a function of μ for varying R of 0.5 km (solid curve), 1.0 km (dashed curve), 2.5 km (solid curve with circles), and 5.0 km (solid curve with triangles). Here, $\lambda_x = 2500$ m, $t = 100$ s, $\alpha = 10.0$ dBZ, and $C = 0.001$ s^{-1}.

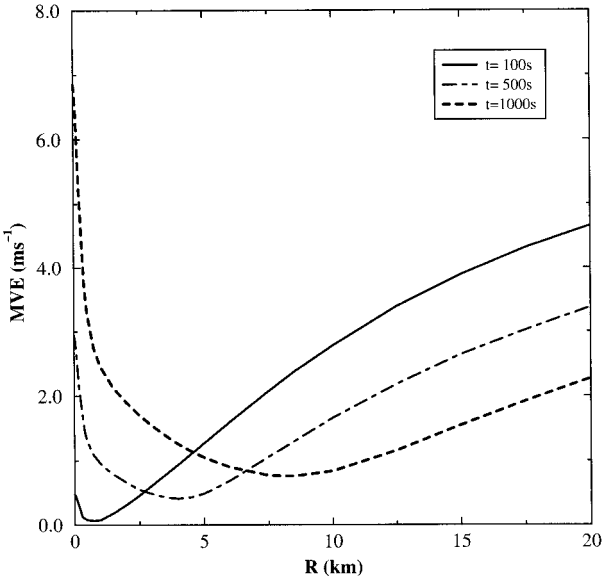

FIG. 11. Divergent flow solution to GZ. Each curve represents the domain MVE as a function of R for varying time integrations of 100 s (solid curve), 500 s (dashed-dotted curve), and 1000 s (dashed curve). Here, $C = 0.001$ s^{-1}, and $\alpha = 10.0$ dBZ. Here, μ is determined from Eq. (3).

appendix A. By inspection of (5) and (6), this includes a_{11}, b_1, and b_2. Substituting the analytic reflectivity field (21) into the expressions for these three coefficients and integrating in space and time, we arrive at the divergent flow solution [see (C1)–(C3) in appendix C for the coefficients].

Figure 10 is a log-linear plot of four curves of varying R for the (error free) divergent flow experiments as a function of weight and MVE defined by (20). Note that a perfect (MVE = 0.0) local flow retrieval implies that $u^r_{i,j} = u(x)$, where $u(x)$ is given by (23), and $v^r_{i,j} = 0$ at each point in the domain. For comparison purposes, the domain is taken to be the same as that specified for the constant wind retrieval in section 4 with horizontal dimensions of 40 km $\times$ 40 km and x and $y > 0$ with respect to the radar. Here, R varies from 0.5 to 5.0 km, λ_x ($=2\pi/k$) = 2500 m, and $t = 100$ s. The divergent flow, ranging from $u = 0.0$ m s^{-1} to $u = -36.4$ m s^{-1} from west to east across the domain (see Fig. 9), was taken to be representative of a strong surface outflow boundary. In direct contrast to the constant wind solution with error, the divergent flow solutions improve (i.e., the MVE decreases) as the weight μ increases. In the absence of error, the reflectivity conservation equation is essential to a successful local flow GZ retrieval. As one might expect, radial velocity information alone is not sufficient to retrieve the *local* velocity field (if it were, then, e.g., the projection of the radial velocity component onto u and v at z = 0 would be sufficient to retrieve the local flow). It is this very limitation that has been the impetus for the development of SDVR techniques involving reflectivity and other conservation principles. The divergent flow solution is quite sensitive to R for $0.01 < \mu < 1000$. However, weights determined via (3) indicate typical values on the order of 1500 m^2 dBZ^{-2} or greater. In practice, weights could be chosen artificially high to avoid any errors resulting from this sensitivity. In doing so, however, there remains the possibility of some undesirable side effects that a more thorough analysis might bring out (e.g., one involving errors in the reflectivity).

The sensitivity of the divergent flow solution with respect to R is shown in Fig. 11. Here we have taken $\lambda_x = 2500$ m, $\alpha = 10$ dBZ, and $C = 0.001$. The three curves represent time integrations of 100, 500, and 1000 s. For increasing R, we retrieve more of the mean (i.e., the domain average) flow than the local flow and, consequently, the MVE increases. The associated R that produces the smallest MVE values varies in each of the three cases and is larger (as is the MVE) for longer integration periods. For perfect data, the best retrieval is achieved by using observations that are more closely spaced in time (i.e., when the assumption of velocity stationarity is least violated). These results also suggest that the choice of an optimal R used to retrieve the local flow may depend upon the time between radar scans. For perfect data and an evolving flow field, one can compensate (somewhat) for the loss of temporal resolution, that

is, an increase in the time between consecutive radar volume scans, by increasing R.

6. Summary and discussion

The sensitivity of the Gal-Chen and Zhang (1993) single-Doppler velocity retrieval to both internal and external parameters was examined. In the first case, we considered the retrieval with a sinusoidal reflectivity pattern that is advected by a mean zonal flow. The second case is identical to the first except that the reflectivity field is assumed to be contaminated with a sinusoidal error term. In the third case the zonal velocity is a linear function of x. For each case a number of parameters was systematically varied, including the signal wavenumber and amplitude and the area of integration. In addition to these variations, different values for the noise wavenumber and amplitude were applied in the second case, while in the third case varying integration time periods (i.e., time between successive radar scans) was examined. The findings for these three cases are summarized below.

1) In the absence of reflectivity or radial velocity errors, the GZ solution for a constant wind is independent of the area of integration R, the radar location (x_0, y_0), signal wavenumber k, and weight μ.
2) In the presence of perfect radial wind information, any error in the reflectivity field degrades the solution for the constant wind case. Consequently, the retrieval performs better without any reflectivity information.
3) For the constant wind with error and divergent flow cases, estimates using (3) indicate that the typical weight is two orders of magnitude greater than values that would impact the solution, suggesting that the GZ scheme is relatively insensitive to changes in μ.
4) In contrast to the error-free constant wind solution, the constant wind with error solution is dependent on R.
5) For given values of α, U, λ_x, and t, the scheme displays similar sensitivity to high amplitude-to-long wavelength noise as it does to low amplitude-to-short wavelength noise.
6) A reduction in the MVE for the divergent (local) flow solution occurs as μ is increased, indicating the importance of reflectivity conservation when seeking the local flow solution.
7) MVE statistics for the local flow solution reveal that there exists an optimal value of R that depends on the time between radar scans. The loss in temporal resolution due to an increase in time between successive volume scans can be offset somewhat by choosing larger values of R.
8) There is an inability to retrieve the mean or local flow in regions where $\mathbf{r} \times \nabla Z = 0$.
9) Of the three test cases, only the divergent-flow solution depends on the radar location (x_0, y_0).

Although the analyses presented in this paper offer some insight regarding the sensitivity of the GZ scheme, real data (or more thorough simulated data studies) offer a far more robust test of single-Doppler velocity retrieval. For example, errors in real data are not necessarily systematic, nor are they generally confined to a single amplitude and wavelength. Heretofore, the GZ method has been applied, using real data, to boundary layer phenomena such as the sea breeze and surface cold pool. In this sense these highly idealized solutions are similar to their real data counterparts, as both do not consider the circumstances under which reflectivity conservation might seriously be violated (e.g., deep convection). Additionally, the assumption of velocity stationarity will likely be violated for rapidly evolving flow fields, especially if the time between successive radar volume scans exceeds the timescale of the local eddies.

It is important to point out that a central tenet of the GZ scheme is its moving frame formulation (GZ96). It was hypothesized by Gal-Chen (1982) that the velocity stationarity assumption is least violated in a frame of reference moving with the principal features of interest. Because a Doppler radar samples the atmosphere at discrete time intervals, finite difference estimates of time derivatives based on these measurements are prone to aliasing. By defining an appropriate moving reference frame, (e.g., one that minimizes the time tendency of reflectivity), one can minimize the impact of errors that result from aliasing. With respect to the cases presented here, the reflectivity time tendency is known perfectly, hence the solutions are presented for a fixed frame only. However, as shown for the divergent flow solution, the velocity stationarity assumption is violated for an evolving flow field. Therefore, extending the study to include a moving frame solution would serve to identify and quantify the sensitivity of GZ to rapidly evolving flow fields as well as detail the advantages of a moving reference frame retrieval under these circumstances.

Acknowledgments. The authors would like to thank Jian Zhang and Stephane Laroche for their input and suggestions. A special note of appreciation is in order for Tzvi Gal-Chen, whose untimely death in 1994 preceded this work. His insight led to the development of the particular SDVR technique investigated herein. The computations were performed on IBM RISC System 6000 in conjunction with computer support from the Center for Analysis and Prediction of Storms (CAPS). This research represents part of the author's Ph.D. thesis at the School of Meteorology, University of Oklahoma, and was supported by the National Science Foundation under Grant ATM91-20009 to CAPS and ATM-92-22576 to the third author.

APPENDIX A

Mean Flow Coefficients

The mean flow coefficients are given as follows:

$$a_{11} = \int_0^t \int_{y-R}^{y+R} \int_{x-R}^{x+R} \left\{ \mu \left(\frac{\partial Z}{\partial x^*} \right)^2 + \left(\frac{x^* - x_0}{r} \right)^2 \right\} dx^*\, dy^*\, dt^*$$

$$= 2\mu\alpha^2 k^2 R^2 t - \frac{R}{2U} \mu\alpha^2 \sin(2kR)\{\sin[2k(x - Ut)] - \sin(2kx)\}$$

$$+ 4R^2 t - \frac{t}{2}\left\{ (y+R)^2 \left[\tan^{-1}\left(\frac{x+R}{y+R} \right) - \tan^{-1}\left(\frac{x-R}{y+R} \right) \right] - (y-R)^2 \left[\tan^{-1}\left(\frac{x+R}{y-R} \right) - \tan^{-1}\left(\frac{x-R}{y-R} \right) \right] \right\}$$

$$- \frac{t}{2}(x+R)\left\{ 2R + (x+R)\left[\tan^{-1}\left(\frac{y-R}{x+R} \right) - \tan^{-1}\left(\frac{y+R}{x+R} \right) \right] \right\}$$

$$+ \frac{t}{2}(x-R)\left\{ 2R + (x-R)\left[\tan^{-1}\left(\frac{y-R}{x-R} \right) - \tan^{-1}\left(\frac{y+R}{x-R} \right) \right] \right\}. \tag{A1}$$

$$a_{12} = \int_0^t \int_{y-R}^{y+R} \int_{x-R}^{x+R} \frac{(x^* - x_0)(y^* - y_0)}{r^2}\, dx^*\, dy^*\, dt^*$$

$$= \frac{t}{4}\left\{ (y+R)^2 \log\left[\frac{(y+R)^2 + (x+R)^2}{(y+R)^2 + (x-R)^2} \right] + (x+R)^2 \log\left[\frac{(y+R)^2 + (x+R)^2}{(y-R)^2 + (x+R)^2} \right] \right.$$

$$\left. + (y-R)^2 \log\left[\frac{(y-R)^2 + (x-R)^2}{(y-R)^2 + (x+R)^2} \right] + (x-R)^2 \log\left[\frac{(y-R)^2 + (x-R)^2}{(y+R)^2 + (x-R)^2} \right] \right\}. \tag{A2}$$

$$a_{22} = \int_0^t \int_{y-R}^{y+R} \int_{x-R}^{x+R} \left(\frac{y^* - y_0}{r} \right)^2 dx^*\, dy^*\, dt^*$$

$$= \frac{t}{2}\left\{ (y+R)^2 \left[\tan^{-1}\left(\frac{x+R}{y+R} \right) - \tan^{-1}\left(\frac{x-R}{y+R} \right) \right] - (y-R)^2 \left[\tan^{-1}\left(\frac{x+R}{y-R} \right) - \tan^{-1}\left(\frac{x-R}{y-R} \right) \right] \right\}$$

$$+ \frac{t}{2}(x+R)\left\{ 2R + (x+R)\left[\tan^{-1}\left(\frac{y-R}{x+R} \right) - \tan^{-1}\left(\frac{y+R}{x+R} \right) \right] \right\}$$

$$- \frac{t}{2}(x-R)\left\{ 2R + (x-R)\left[\tan^{-1}\left(\frac{y-R}{x-R} \right) - \tan^{-1}\left(\frac{y+R}{x-R} \right) \right] \right\}. \tag{A3}$$

$$a_{13} = a_{31} = 0 \qquad a_{21} = a_{12}, \qquad a_{23} = a_{32} = 0, \quad \text{and} \quad a_{33} = 0. \tag{A4}$$

$$b_1 = \int_0^t \int_{y-R}^{y+R} \int_{x-R}^{x+R} \left(-\mu \frac{\partial Z}{\partial x^*} \frac{\partial Z}{\partial t^*} + v_r \frac{x^* - x_0}{r} \right) dx^*\, dy^*\, dt^* = U \times a_{11}. \tag{A5}$$

$$b_2 = \int_0^t \int_{y-R}^{y+R} \int_{x-R}^{x+R} \left(-\mu \frac{\partial Z}{\partial y^*} \frac{\partial Z}{\partial t^*} + v_r \frac{y^* - y_0}{r} \right) dx^*\, dy^*\, dt^* = U \times a_{12}. \tag{A6}$$

An asterisk indicates a dummy variable; r, R, and (x_0, y_0) are given in Fig. 1; and $v_r = U(x - x_0/r)$.

APPENDIX B

Mean Flow Error Coefficients

The following two terms are added onto Eqs. (A1) and (A5), respectively. All other coefficients remain the same as defined in appendix A.

$$\varepsilon_{a_{11}} = \int_0^t \int_{y-R}^{y+R} \int_{x-R}^{x+R} \mu \left[2 \frac{\partial \varepsilon}{\partial x^*} \frac{\partial Z}{\partial x^*} \bigg|_{\varepsilon=0} + \left(\frac{\partial \varepsilon}{\partial x^*} \right)^2 \right] dx^* \, dy^* \, dt^*$$

$$= 2\mu R^2 \beta^2 m^2 t + \frac{\mu R t \beta^2 m}{2} \{\sin[2m(x+R)] - \sin[2m(x-R)]\}$$

$$+ \frac{2\mu\alpha\beta m R}{(m+k)U} \sin(kUt) \{\sin[(m+k)(x+R)] - \sin[(m+k)(x-R)]\}$$

$$+ \frac{2\mu\alpha\beta m R}{(m-k)U} \sin(kUt) \{\sin[(m-k)(x+R)] - \sin[(m-k)(x-R)]\}$$

$$+ \frac{2\mu\alpha\beta m R}{(m+k)U} [\cos(kUt) - 1] \{\cos[(m+k)(x+R)] - \cos[(m+k)(x-R)]\}$$

$$+ \frac{2\mu\alpha\beta m R}{(k-m)U} [\cos(kUt) - 1] \{\cos[(k-m)(x+R)] - \cos[(k-m)(x-R)]\}. \quad \text{(B1)}$$

$$\varepsilon_{b_1} = \int_0^t \int_{y-R}^{y+R} \int_{x-R}^{x+R} -\mu \frac{\partial Z}{\partial t^*} \frac{\partial \varepsilon}{\partial x^*} \, dx^* \, dy^* \, dt^*$$

$$= \frac{\mu\alpha\beta m R}{(m+k)} \sin(kUt) \{\sin[(m+k)(x+R)] - \sin[(m+k)(x-R)]\}$$

$$+ \frac{\mu\alpha\beta m R}{(m-k)} \sin(kUt) \{\sin[(m-k)(x+R)] - \sin[(m-k)(x-R)]\}$$

$$+ \frac{\mu\alpha\beta m R}{(m+k)} [\cos(kUt) - 1] \{\cos[(m+k)(x+R)] - \cos[(m+k)(x-R)]\}$$

$$+ \frac{\mu\alpha\beta m R}{(k-m)} [\cos(kUt) - 1] \{\cos[(k-m)(x+R)] - \cos[(k-m)(x-R)]\}. \quad \text{(B2)}$$

APPENDIX C

Divergent Flow Coefficients

Here, $a_{11}(Z)$, shown below, denotes the solution associated with the portion of a_{11} integrand given by the $\partial Z/\partial x$ term and, when substituted in place of the first two terms on the right-hand side of (A1), yields the divergent flow a_{11}.

$$a_{11}(Z) = \int_0^t \int_{y-R}^{y+R} \int_{x-R}^{x+R} \mu \left(\frac{\partial Z}{\partial x^*} \right) dx^* \, dy^* \, dt^*$$

$$= \frac{R}{4C(x+R)} \mu\alpha^2 \{\cos[2k(x+R)] - (1+Ct)\cos[2k(x+R)(1+Ct)]\}$$

$$+ \frac{R}{4C(x-R)} \mu\alpha^2 \{(1+Ct)\cos[2k(x-R)(1+Ct)] - \cos[2k(x-R)]\}$$

$$+ \frac{R}{8Ck(x+R)^2} \mu\alpha^2 \{\sin[2k(x+R)(1+Ct)] - \sin[2k(x+R)]\}$$

$$+ \frac{R}{8Ck(x-R)^2} \mu\alpha^2 \{\sin[2k(x-R)] - \sin[2k(x-R)(1+Ct)]\} + \frac{2\mu\alpha^2 k^2 R^2}{3C} [(1+Ct)^3 - 1]. \quad \text{(C1)}$$

All other coefficients are given in appendix A, with the exception of the following:

$$b_1 = \int_0^t \int_{y-R}^{y+R} \int_{x-R}^{x+R} \left(-\mu \frac{\partial z}{\partial x^*} \frac{\partial z}{\partial t^*} + v_r \frac{x^* - x_0}{r} \right) dx^*\, dy^*\, dt^*$$

$$= \int_0^t \int_{y-R}^{y+R} \int_{x-R}^{x+R} \left\{ \mu\alpha^2 k^2 C x^* \cos^2[kx^*(1 + Ct^*)] - \frac{C(x^* - x_0)^2 x^*}{r^2(1 + Ct^*)} \right\} dx^*\, dy^*\, dt^*$$

$$= \mu\alpha^2 R^2 x k^2 [1 - (1 + Ct)^2] - 4R^2(x + x_0)\log(1 + Ct)$$

$$+ \frac{\mu\alpha^2 R}{4}\{\cos[2k(x + R)(1 + Ct)] - \cos[2k(x + R)] - \cos[2k(x - R)(1 + Ct)] + \cos[2k(x - R)]\}$$

$$\times \left\{ \log|2k(x + R)(1 + Ct)| - \log|2k(x + R)| - \frac{[2k(x + R)(1 + Ct)]^2}{2(2!)} \right.$$

$$\left. + \frac{[2k(x + R)]^2}{2(2!)} + \frac{[2k(x + R)(1 + Ct)]^4}{4(4!)} - \frac{[2k(x + R)]^4}{4(4!)} + \text{HOT} \right\}$$

$$+ \frac{\mu\alpha^2 R}{4} \left\{ \log|2k(x - R)(1 + Ct)| - \log|2k(x - R)| - \frac{[2k(x - R)(1 + Ct)]^2}{2(2!)} \right.$$

$$\left. + \frac{[2k(x - R)]^2}{2(2!)} + \frac{[2k(x - R)(1 + Ct)]^4}{4(4!)} - \frac{[2k(x - R)]^4}{4(4!)} + \text{HOT} \right\}$$

$$+ \frac{\log(1 + Ct)}{6} \left\{ 16xR^2 + (y + R)^3 \log\left[\frac{(y + R)^2 + (x + R)^2}{(y + R)^2 + (x - R)^2}\right] + (y - R)^3 \log\left[\frac{(y - R)^2 + (x - R)^2}{(y - R)^2 + (x + R)^2}\right] \right.$$

$$\left. + 2(x + R)^3 \left[\tan^{-1}\left(\frac{y - R}{x + R}\right) - \tan^{-1}\left(\frac{y + R}{x + R}\right)\right] - 2(x - R)^3 \left[\tan^{-1}\left(\frac{y - R}{x - R}\right) - \tan^{-1}\left(\frac{y + R}{x - R}\right)\right] \right\}$$

$$+ \frac{x_0}{2} \log(1 + Ct) \left\{ 4R^2 + (y + R)^2 \left[\tan^{-1}\left(\frac{x + R}{y + R}\right) - \tan^{-1}\left(\frac{x - R}{y + R}\right)\right] - (y - R)^2 \left[\tan^{-1}\left(\frac{x + R}{y - R}\right) + \tan^{-1}\left(\frac{x - R}{y - R}\right)\right] \right.$$

$$\left. - (x + R)^2 \left[\tan^{-1}\left(\frac{y + R}{x + R}\right) - \tan^{-1}\left(\frac{y - R}{x + R}\right)\right] + (x - R)^2 \left[\tan^{-1}\left(\frac{y + R}{x - R}\right) - \tan^{-1}\left(\frac{y - R}{x - R}\right)\right] \right\}, \tag{C2}$$

where ''HOT'' is the higher-order terms of the series expansion and

$$b_2 = \int_0^t \int_{y-R}^{y+R} \int_{x-R}^{x+R} v_r \frac{y^* - y_0}{r}\, dx^*\, dy^*\, dt^* = \int_0^t \int_{y-R}^{y+R} \int_{x-R}^{x+R} -\frac{C(x^* - x_0)(y^* - y_0)x^*}{r^2(1 + Ct^*)}\, dx^*\, dy^*\, dt^*$$

$$= \log(1 + Ct) \left(-4yR^2 + \frac{1}{3} \left[(y + R)^3 \tan^{-1}\left(\frac{x + R}{y + R}\right) - (y - R)^3 \tan^{-1}\left(\frac{x + R}{y - R}\right) \right.\right.$$

$$\left.\left. - (y + R)^3 \tan^{-1}\left(\frac{x - R}{y + R}\right) - (y - R)^3 \tan^{-1}\left(\frac{x - R}{y - R}\right)\right] \right.$$

$$+ \frac{(x + R)}{6} \left\{ 4Ry + (x + R)^2 \log\left[\frac{(y - R)^2 + (x + R)^2}{(y + R)^2 + (x + R)^2}\right] \right\}$$

$$- \frac{(x - R)}{6} \left\{ 4Ry + (x - R)^2 \log\left[\frac{(y - R)^2 + (x - R)^2}{(y + R)^2 + (x - R)^2}\right] \right\}$$

$$+ \frac{x_0}{4}(x + R)^2 \log\left[\frac{(x + R)^2 + (y - R)^2}{(x + R)^2 + (y + R)^2}\right] + \frac{x_0}{4}(y + R)^2 \log\left[\frac{(x - R)^2 + (y + R)^2}{(x + R)^2 + (y + R)^2}\right]$$

$$\left. + \frac{x_0}{4}(y - R)^2 \log\left[\frac{(x + R)^2 + (y - R)^2}{(x - R)^2 + (y - R)^2}\right] + \frac{x_0}{4}(x - R)^2 \log\left[\frac{(x - R)^2 + (y + R)^2}{(x - R)^2 + (y - R)^2}\right] \right). \tag{C3}$$

REFERENCES

Crook, A., 1994: Numerical simulations initialized with radar-derived winds. Part I: Simulated data experiments. *Mon. Wea. Rev.,* **122,** 1189–1203.

——, and J. D. Tuttle, 1994: Numerical simulations initialized with radar-derived winds. Part II: Forecasts of three gust front cases. *Mon. Wea. Rev.,* **122,** 1204–1217.

Gal-Chen, T., 1978: A method for the initialization of the anelastic equations: Implications for matching models with observations. *Mon. Wea. Rev.,* **106,** 587–606.

——, 1982: Errors in fixed and moving frame of references: Applications for conventional and Doppler radar analysis. *J. Atmos. Sci.,* **39,** 2279–2300.

——, and J. Zhang, 1993: On the optimal use of reflectivities and single-Doppler radar velocities to deduce 3D motions. Preprints, *26th Int. Conf. on Radar Meteorology,* Norman, OK, Amer. Meteor. Soc., 414–416.

Hane, C. E., R. B. Wilhelmson, and T. Gal-Chen, 1981: Retrieval of thermodynamic variables within deep convective clouds: Experiments in three dimensions. *Mon. Wea. Rev.,* **109,** 564–576.

Liou, Y. C., T. Gal-Chen, and D. K. Lilly, 1991: Retrievals of wind, temperature, and pressure from single-Doppler radar and a numerical model. Preprints, *25th Int. Conf. on Radar Meteorology,* Paris, France, Amer. Meteor. Soc., 151–154.

Qiu, C.-J., and Q. Xu, 1992: A simple adjoint method of wind analysis for single-Doppler data. *J. Atmos. Oceanic Technol.,* **9,** 588–598.

Shapiro, A., S. Ellis, and J. Shaw, 1995: Single-Doppler velocity retrievals with Phoenix II data: Clear air and microburst wind retrievals in the planetary boundary layer. *J. Atmos. Sci.,* **52,** 1265–1287.

Sun, J., 1994: Fitting a Cartesian prediction model to radial velocity from single-Doppler radar. *J. Atmos. Oceanic Technol.,* **11,** 200–204.

——, and A. Crook, 1994: Wind and thermodynamic retrieval from single-Doppler measurements of a gust front observed during Phoenix II. *Mon. Wea. Rev.,* **122,** 1075–1091.

——, and ——, 1996: Comparison of thermodynamic retrieval by the adjoint method with the traditional retrieval method. *Mon. Wea. Rev.,* **124,** 308–324.

——, D. W. Flicker, and D. K. Lilly, 1991: Recovery of three-dimensional wind and temperature fields from simulated single-Doppler radar data. *J. Atmos. Sci.,* **48,** 876–890.

Tuttle, J. D., and G. B. Foote, 1990: Determination of the boundary layer airflow from a single-Doppler radar. *J. Atmos. Oceanic Technol.,* **7,** 218–232.

Weygandt, S., A. Shapiro, and K. K. Droegemeier, 1995: Adaptation of a single-Doppler velocity retrieval on a deep-convective storm. Preprints, *27th Conf. on Radar Meteorology,* Vail, CO, Amer. Meteor. Soc., 264–266.

Xu, Q., C.-J. Qiu, and J.-X. Yu, 1994: Adjoint-method retrievals of low-altitude wind fields from single-Doppler reflectivity measured during Phoenix II. *J. Atmos. Oceanic Technol.,* **11,** 275–288.

——, ——, H.-D. Gu, and J.-X. Yu, 1995: Simple adjoint retrievals of microburst winds from single-Doppler radar data. *Mon. Wea. Rev.,* **123,** 1822–1833.

Zhang, J., and T. Gal-Chen, 1996: Single-Doppler wind retrieval in the moving frame of reference. *J. Atmos. Sci.,* **53,** 2609–2623.